



Absorption Troughs of Ly α Emitters in HETDEX

Laurel H. Weiss¹, Dustin Davis¹, Karl Gebhardt¹, Simon Gazagnes¹, Mahan Mirza Khanlari¹, Erin Mentuch Cooper¹, John Chisholm¹, Danielle Berg¹, William P. Bowman², Chris Byrohl³, Robin Ciardullo^{4,5}, Maximilian Fabricius^{6,7}, Daniel Farrow^{8,9}, Caryl Gronwall^{4,5}, Gary J. Hill^{1,10}, Lindsay R. House^{1,17}, Donghui Jeong^{4,5}, Hasti Khoraminezhad¹¹, Wolfram Kollatschny¹², Eiichiro Komatsu^{13,14,15}, Maja Lujan Niemeyer¹³, Shun Saito^{11,15}, Donald P. Schneider^{4,5}, and Gregory R. Zeimann¹⁶

¹ Department of Astronomy, The University of Texas at Austin, 2515 Speedway Boulevard, Stop C1400, Austin, TX 78712, USA

² Department of Astronomy, Yale University, New Haven, CT 06511, USA

³ Universitäts Heidelberg, Zentrum für Astronomie, Institut für Theoretische Astrophysik, Albert-Ueberle-Str. 2, D-69120 Heidelberg, Germany

⁴ Department of Astronomy & Astrophysics, The Pennsylvania State University, University Park, PA 16802, USA

⁵ Institute for Gravitation and the Cosmos, The Pennsylvania State University, University Park, PA 16802, USA

⁶ Max-Planck-Institut für Extraterrestrische Physik, Gießenbachstraße 1, D-85748 Garching, Germany

⁷ Universitäts-Sternwarte München, Scheinerstraße 1, D-81679 München, Germany

⁸ Centre of Excellence for Data Science, Artificial Intelligence & Modeling (DAIM), University of Hull, Cottingham Road, Hull, HU6 7RX, UK

⁹ E.A. Milne Centre for Astrophysics University of Hull, Cottingham Road, Hull, HU6 7RX, UK

¹⁰ McDonald Observatory, The University of Texas at Austin, 2515 Speedway Boulevard, Stop C1402, Austin, TX 78712, USA

¹¹ Institute for Multi-messenger Astrophysics and Cosmology, Department of Physics, Missouri University of Science and Technology, 1315 N Pine Street, Rolla, MO 65409, USA

¹² Institut für Astrophysik und Geophysik, Universität Göttingen, Friedrich-Hund Platz 1, D-37077 Göttingen, Germany

¹³ Max-Planck-Institut für Astrophysik, Karl-Schwarzschild-Str. 1, D-85741 Garching, Germany

¹⁴ Ludwig-Maximilians-Universität München, Schellingstr. 4, D-80799 München, Germany

¹⁵ Kavli Institute for the Physics and Mathematics of the Universe (Kavli IPMU, WPI), University of Tokyo, Chiba 277-8582, Japan

¹⁶ Hobby–Eberly Telescope, University of Texas, Austin, TX 78712, USA

Received 2023 October 12; revised 2023 December 7; accepted 2024 January 3; published 2024 February 12

Abstract

The Hobby–Eberly Telescope Dark Energy Experiment (HETDEX) is designed to detect and measure the redshifts of more than 1 million Ly α emitting galaxies (LAEs) $1.88 < z < 3.52$. In addition to its cosmological measurements, these data enable studies of Ly α spectral profiles and the underlying radiative transfer. Using the roughly half a million LAEs in the HETDEX Data Release 3, we stack various subsets to obtain the typical Ly α profile for the $z \sim 2$ – 3 epoch and to understand their physical properties. We find clear absorption wings around Ly α emission, which extend $\sim 2000 \text{ km s}^{-1}$ both redward and blueward of the central line. Using far-UV spectra of nearby ($0.002 < z < 0.182$) LAEs in the COS Legacy Archive Spectroscopic Survey treasury and optical/near-IR spectra of $2.8 < z < 6.7$ LAEs in the Multi Unit Spectroscopic-Wide survey, we observe absorption profiles in both redshift regimes. Dividing the sample by volume density shows that the troughs increase in higher-density regions. This trend suggests that the depth of the absorption is dependent on the local density of objects near the LAE, a geometry that is similar to damped Ly α systems. Simple simulations of Ly α radiative transfer can produce similar troughs due to absorption of light from background sources by HI gas surrounding the LAEs.

Unified Astronomy Thesaurus concepts: High-redshift galaxies (734); Ly α galaxies (978); Diffuse radiation (383)

1. Introduction

The Ly α emission line has long been regarded as a powerful tool with which to probe galaxies in the act of formation (Partridge & Peebles 1967). As expected, Ly α emitters (LAEs) have become one of the most heavily observed components of the high-redshift Universe, being identified as early as $z > 7$ with the JWST (e.g., Tang et al. 2023). The Ly α emission line is useful because it is easily detectable via narrowband imaging or spectroscopy (see Ouchi et al. 2020, for a review). As a result, ground-based observations can use LAEs to trace the large-scale structure of galaxies from $z \sim 1.8$ to $z \sim 6.5$. Detecting this feature is the primary goal of the Hobby–Eberly

Telescope Dark Energy experiment (HETDEX; Gebhardt et al. 2021; Hill et al. 2021). Using LAEs, HETDEX aims to measure the $z \sim 2.4$ Hubble expansion rate, $H(z)$, and the angular diameter distance, $D_A(z)$, by identifying and 3D mapping over 1 million LAEs (Gebhardt et al. 2021).

Given the importance of LAEs in the study of the early Universe, it is essential that we understand their physical properties and the physics behind their Ly α emission. Since Ly α is a resonance line, its radiative transfer is complicated and results in a variety of observed Ly α spectral profiles (Verhamme et al. 2006). The fate of Ly α photons depends on the geometry and physical conditions of not only the interstellar medium (ISM), but also the circumgalactic medium (CGM) and the intergalactic medium (IGM). After its production via photoionization, a Ly α photon’s escape from the ISM is dependent on the amount and distribution of dust (e.g., Finkelstein et al. 2008; Scarlata et al. 2009; Schaerer et al. 2011), ISM kinematics (e.g., Kunth et al. 1998), and the galaxy’s neutral gas content and geometry (e.g., Neufeld 1991;

¹⁷ NSF Graduate Research Fellow.

Hansen & Oh 2006; Jaskot & Oey 2014). Beyond the ISM and out to the galaxy’s virial radius, Ly α photons resonantly scatter throughout the CGM.

Observationally, the CGM has been detected in extended Ly α emission as Ly α halos (e.g., Steidel et al. 2010; Matsuda et al. 2012; Wisotzki et al. 2016), as well as in Ly α absorption from foreground/background galaxy pairs (Steidel et al. 2010). Studies aimed at modeling Ly α in the CGM suggest that the gas is multiphase with complex kinematics (e.g., Dijkstra & Kramer 2012; Shen et al. 2013; Chung et al. 2019). For example, inflows and outflows can have a strong effect on the Ly α profile shape (e.g., Park et al. 2021).

Outside the virial radius, photons must traverse the IGM. This reservoir of gas resides in filaments between galaxies, tracing structures on megaparsec (Mpc) scales. In the rest frame of the intervening gas, photons at the Ly α wavelength are readily absorbed/scattered, and this has long been observed along lines of sight to bright quasars as the Ly α forest (e.g., Gunn & Peterson 1965; Lynds 1971; Hu et al. 1995; Slosar et al. 2011). The physical properties of the ISM, CGM, and IGM are naturally encoded within an observed Ly α profile, although the constraints on their influence are not yet fully developed.

The HETDEX is an untargeted spectroscopic survey, using integral field unit (IFU) spectroscopy to detect and measure the redshift of Ly α from $z \sim 1.88$ to 3.52 galaxies. The more than 1 million LAE spectra expected from HETDEX provide the opportunity to investigate Ly α emission in the context of a variety of properties. There has been a wealth of observations of Ly α in both the local (e.g., Kunth et al. 1998; Cowie et al. 2010; Rivera-Thorsen et al. 2015; Berg et al. 2022) and high-redshift Universe (e.g., Ouchi et al. 2008; Stark et al. 2010; Shibuya et al. 2012; Urrutia et al. 2019). Comparisons of HETDEX LAEs to spectra of LAEs at lower and higher redshifts provide an opportunity to investigate the profile of Ly α in LAEs across cosmic time, and, by extension, to investigate key aspects of galaxy evolution. Furthermore, an understanding of the profiles of Ly α helps HETDEX discriminate between true LAEs and false detections, and thereby reduce the measurement error on $H(z)$ and $D_A(z)$.

While the individual exposure time in HETDEX of ~ 18 minutes on source does not provide sufficient signal-to-noise ratio (S/N) to investigate the detailed structure of the Ly α profile for an individual LAE, we can stack the spectra of the survey’s ~ 1 million LAEs to greatly enhance the signal. Given the size and breadth of the sample, we can explore the stacks according to physical properties such as redshift, mass, and environment.

This paper is organized as follows. Section 2 introduces LAE data sets from HETDEX, the COS Legacy Archive Spectroscopic Survey (CLASSY; Berg et al. 2022), and the Multi Unit Spectroscopic (MUSE)-Wide survey (Bacon et al. 2010). Section 3 presents the stacking methodology. Section 4 discusses the analysis of these stacks, and Section 5 discusses a physical interpretation of our results. Throughout the paper, we will assume a Planck 2018 cosmology (Planck Collaboration I 2020) with $\Omega_m = 0.31$ and $H_0 = 67.7 \text{ km s}^{-1} \text{ Mpc}^{-1}$. All magnitudes are in the AB system (Oke & Gunn 1983).

2. Optical and UV Spectroscopy

The HETDEX (Gebhardt et al. 2021; Hill et al. 2021) is a multiyear, untargeted spectroscopic survey conducted with the

upgraded Hobby–Eberly Telescope (HET; Ramsey et al. 1998; Hill et al. 2021). The HETDEX instrument is the Visible Integral-Field Replicable Unit Spectrograph (VIRUS; Hill et al. 2018, 2021). VIRUS consists of 78 IFUs and 156 spectrographs, where each IFU covers $51'' \times 51''$ on the sky. Each IFU contains 448 1.5 diameter optical fibers, which feed a pair of low-resolution ($750 < R < 950$) spectrographs covering the wavelength range between 3500 and 5500 Å. The fibers in a given IFU are spaced to give a one-third fill factor, so that a three-position dithered set of exposures provides full spatial coverage within an IFU (Hill et al. 2021). The typical exposure time of ~ 18 minutes over three dithers then provides $3 \times 34,944$ spectra.

The processing of HETDEX frames is described in detail in Gebhardt et al. (2021). The spectra are calibrated, sky subtracted, and inspected for emission lines and continuum sources. If an object is detected in a fiber, a point-spread-function (PSF) weighted spectrum is extracted from the surrounding fibers. The PSF-weighted spectra are then classified and their redshifts are determined with the ELiXer software package (Davis et al. 2023b).

With the exception of the stack from the HETDEX Public Source Catalog (HPSC-1; see Mentuch Cooper et al. 2023 and Davis et al. 2023a), the LAE spectra in this project come from HETDEX Internal Data Release 3.0.1 (HDR3). This release contains all HETDEX data from 2017 January 3, up to and including 2021 August 3. The updated source catalog contains (at $S/N > 5$) $\sim 520,000$ LAEs. In this paper, we select a set of $\sim 300,000$ spectra from this sample, which have high-confidence LAE classifications from ELiXer ($P_{\text{Ly}\alpha} > 0.8$). We then further restrict the LAE sample to objects with emission-line detections with $S/N > 5$ and line widths of $\sigma < 5.5 \text{ \AA}$ ($\sim 350 \text{ km s}^{-1}$); this removes potential active galactic nuclei (AGNs) that were not identified as such by ELiXer or cataloged in Liu et al. (2022).

To compare our LAE spectra to other surveys at low and high redshift, we make use of the CLASSY and MUSE-Wide surveys. Berg et al. (2022) present the high-resolution ($R \sim 15,000$), far-UV (900–2000 Å) CLASSY spectra and the high-level data products from the Cosmic Origins Spectrograph (COS) on the Hubble Space Telescope. The sample of 45 galaxies was chosen to be star-forming, compact (near-UV FWHM $< 2''.5$), low redshift ($z < 0.2$), and UV bright ($m_{\text{FUV}} < 20$). For further discussion on data reduction, extraction, flux calibration, and coaddition of the CLASSY Treasury, see Berg et al. (2022).

The MUSE (Bacon et al. 2010) IFU spectrograph on the Very Large Telescope produces $R \sim 2000$ –4000 optical spectra (4700–9300 Å) over a $1' \times 1'$ field of view. MUSE-Wide is a blind spectroscopic survey that covers 100×1 arcmin² target fields, with a total survey volume in Ly α that amounts to $\sim 10^6 \text{ Mpc}^3$. The first 44 pointings taken in the CANDELS/GOODS-S and CANDELS/COSMOS regions are presented in Urrutia et al. (2019). This sample consists of 479 non-AGN LAEs with Ly α -based redshifts $2.9 < z < 6.3$. For LAEs with cataloged photometric counterparts, they reported spectral energy distribution (SED)-determined mass estimates of $7.5 \lesssim \log (M/M_\odot) \lesssim 10$. More information about the MUSE-Wide observations and sample can be found in Urrutia et al. (2019).

3. Spectral Stacking

Our goal is to use high-S/N spectra around the Ly α line to explore the physical properties of LAEs. This can only be done by stacking; at $z \gtrsim 2$, individual Ly α detections lack the S/N required for such an analysis. Our input sample includes 300,000 LAEs over a redshift range $1.88 < z < 3.52$. The individual spectra are flux calibrated to about 5% accuracy by the HETDEX project (Gebhardt et al. 2021). However, at the extremely faint flux levels that stacking provides, we require additional calibrations to the baseline reductions, including both sky subtraction and flux corrections. The sky subtraction, additional flux calibrations, wavelength shifts, and stacking procedures are described below (see also Gebhardt et al. 2021).

3.1. Additional Corrections for Stacking Analyses

Prior to stacking, we perform several corrections to the processed spectra. As a first step, we use sky residuals to provide a better estimate of the sky. The sky-subtraction procedure removes extraneous light from an object’s spectrum that is due to the atmosphere, foreground/background sources, and/or instrumental effects. For a given observation, HETDEX measures the sky both using the full 21’ diameter focal plane (all 34,944 fibers), and using the local fibers within the immediate vicinity of the detection. We use the latter for this work. This local sky subtraction is based upon an individual amplifier (112 fibers), corresponding to an on-sky region of $50'' \times 12''.5$. We remove fibers with continuum that have more than $3 \times$ the biweight scale (Beers et al. 1990) of the fibers on the amplifier. Significantly extended, diffuse flux associated with a source detection can be removed using the local sky subtraction. For a more detailed description of HETDEX sky subtraction, see Gebhardt et al. (2021). This procedure provides our initial sky-subtracted spectra for all fibers.

Since the act of stacking pushes the flux limit of our data far below the level of the background sky, we must check sky residuals and apply any corrections to the initial analysis, as described in Davis et al. (2023a). For each field, we generate 200 random aperture spectra from regions of the empty sky and stack them using a biweight (Beers et al. 1990). We define our empty sky apertures such that (i) none of the 200 sky regions is within $1''.5$ of each other, (ii) each region contains at least 15 fibers, (iii) the measured g magnitude in the PSF-weighted spectra is fainter than 24, and (iv) there are no detected sources within $2''$. This residual stack is subtracted from the observed-frame fiber spectra of a detection. This subtraction accounts for small calibration corrections, including flux from faint background and foreground sources. For an individual spectrum, this correction is less than 1% of the original sky, far below the typical noise level, and the effect only becomes significant when stacking hundreds or thousands of HETDEX spectra.

After applying this correction, the observed air wavelengths are corrected to vacuum via Greisen et al. (2006), and the spectra are shifted to the rest frame using their redshifts as determined by HETDEX (Mentuch Cooper et al. 2023). Since the reported redshifts are measured from Ly α alone, they do not account for any Ly α velocity offset from the source’s systemic redshift. For parts of this paper, we only correct the wavelengths for redshift, but do not apply any further corrections to the fluxes (such as cosmological dimming, Milky Way dust extinction, etc.). We will discuss the reasons for this approach shortly. We do note that stacking observed

fluxes at different redshifts slightly biases the stack toward lower-redshift objects, as comparatively more flux from these sources contributes, due to less cosmological dimming. Thus, when possible, we convert the observed flux densities to luminosity densities prior to stacking to reduce this bias.

3.2. Stacking Methodology

By stacking hundreds to thousands of spectra, we significantly increase the S/N of detections, and greatly improve our ability to identify and measure weak spectral features. In the case of HETDEX spectra, the stacking of LAEs creates an “average” Ly α profile with an increase in S/N that is roughly proportional to the square root of the number of sources. Moreover, by creating subsamples of galaxies based on the system’s physical properties, we can investigate the systematics of Ly α as a function of parameters such as continuum magnitude and emission-line strength. Since HETDEX is an untargeted survey with hundreds of thousands of spectra currently available, sufficiently large stacks of LAEs average over orientations, environment, geometries, and lines of sight.

We use the stacking method described in Davis et al. (2021) and Davis et al. (2023a). The extent of the rest-frame wavelength coverage is determined from the highest- and lowest-redshift objects to be stacked, with a grid spacing adopted from the highest-redshift object (0.44 \AA for $z = 3.5$). We linearly interpolate the individual rest-frame spectra onto this grid and stack each wavelength bin using a weighted biweight. The weighting scheme is a modified version of Tukey’s biweight estimator (Andrews et al. 1972; Beers et al. 1990) where each point is weighted by the inverse of the flux variance (Davis et al. 2021). For large stacks of more than ~ 1000 spectra, using the mean, median, biweight, and weighted biweight statistics shows little difference (Davis et al. 2023a).

Figure 1 depicts the stack of $\sim 50,000$ HETDEX LAEs from HPSC-1 presented in Davis et al. (2023a). Some of the most prominent features in the spectrum are the significant absorption troughs on either side of the Ly α emission. These troughs, as well as their properties and possible physical origin, are discussed in the following sections. Aside from Ly α , many other spectral features are noticeable in the average stack. While Ly α is visible in individual HETDEX spectra, faint emission and absorption lines, including the Lyman series, become apparent in a stack of many spectra. For a further detailed analysis of this stack, including the SED fitting and derived properties, see Davis et al. (2023a).

4. Ly α Absorption Troughs

Perhaps the most striking feature in Figure 1 is the deep absorption troughs blueward and redward of the Ly α emission. The existence of both Ly α absorption and emission in the spectra of $z \sim 2.5$ LAEs is not unexpected; for example, Erb et al. (2014), Trainor et al. (2015), and Trainor et al. (2019) have all observed LAEs with Ly α absorption primarily blueward of the emission (see Figures 3, 19, and 1 of those studies, respectively). Another example of this combined Ly α profile is the damped Ly α system (DLA) at $z = 2.0395$ presented in Møller et al. (2004). As in the case of the stacked spectrum shown in Figure 1, the 2D spectrum of the DLA displays Ly α emission directly centered in an absorption well (see Figure 1 of Møller et al. 2004). We will revisit DLAs in the

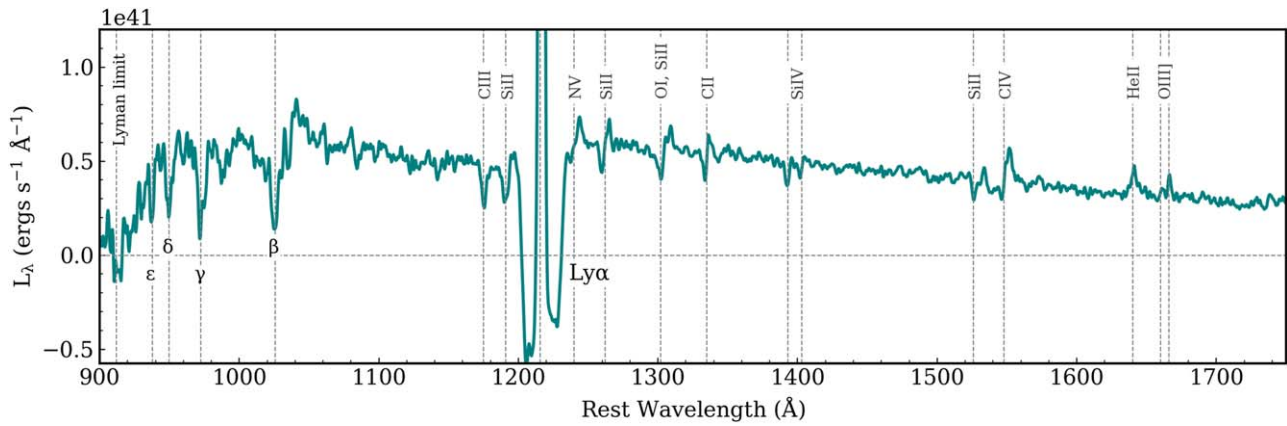


Figure 1. A stack of $\sim 50,000$ high-confidence LAE spectra from HPSC-1, as presented in Davis et al. (2023a). We select the spectra that have a $\text{Ly}\alpha$ line width $\sigma < 5.5 \text{ \AA}$. Faint emission and absorption lines are marked and labeled. While $\text{Ly}\alpha$ emission is detected in individual HETDEX spectra, the other faint emission/absorption features only become visible in stacks of $\gtrsim 10,000$ sources. The significantly negative flux values of the $\text{Ly}\alpha$ absorption troughs are likely the result of background oversubtraction as discussed in text, i.e., the absorption troughs are real, while their negative fluxes result from our assumptions in sky subtraction.

context of HETDEX LAEs in Section 5. We argue below that the existence of the absorption troughs is *not* the result of instrumental/algorithmic effects, as the feature is present in a variety of HETDEX spectral stacks and in other data sets.

4.1. Instrumental and Algorithmic Concerns

The absorption troughs in Figure 1 are significantly broad, sharp and, concerningly, negative. Before we can begin to analyze the shape, evolution, and/or physical origins of the troughs, we must first conclude that they are not due to instrumental or algorithmic effects in HETDEX calibration and data processing. The sources of a systematic error we consider are (i) sky subtraction residuals, (ii) problems with the detectors, (iii) extended $\text{Ly}\alpha$ emission, and (iv) odd and plentiful false-positive behavior.

The HETDEX sky-subtraction algorithm assumes that the instrumental resolving power is the same over all fibers in an amplifier. A systematic trend in the resolving power of the fibers from the center to the edge of the detector could create correlated residuals. For example, subtraction of a bright emission line, if not properly modeled across the detector, could create false absorption wings. However, this residual would result in wings of about one wavelength pixel, while the trough widths we observe are roughly 35 pixels wide. Furthermore, if this residual were the cause, a brighter line would create deeper absorption wings, which is not the case (see Section 4.3). More importantly, this effect would manifest itself in any emission line, and we do not observe the troughs in the detections of $[\text{O II}] \lambda 3727$ or other emission lines detected in HETDEX (see Figure 2).

Another possibility lies in the detector electronics, where a charge transfer could cause a systematic oversubtraction. This effect is signal dependent, detector dependent, asymmetric in wavelength, and far too weak to affect approximately 35 pixels similarly on the 156 detectors. As stated above, this would be present in all detected emission lines, not just $\text{Ly}\alpha$.

Alternatively, the $\text{Ly}\alpha$ absorption troughs observed in the stacked spectra of LAEs may be the manifestation of faint, extended $\text{Ly}\alpha$ emission distributed over most of an IFU's $50''$ field of view. If such halos exist, the local sky estimator employed by HETDEX could cause the line profile of a LAE's halo to be subtracted from the profile of its core. This could produce the profile seen in Figure 1. However, while extended

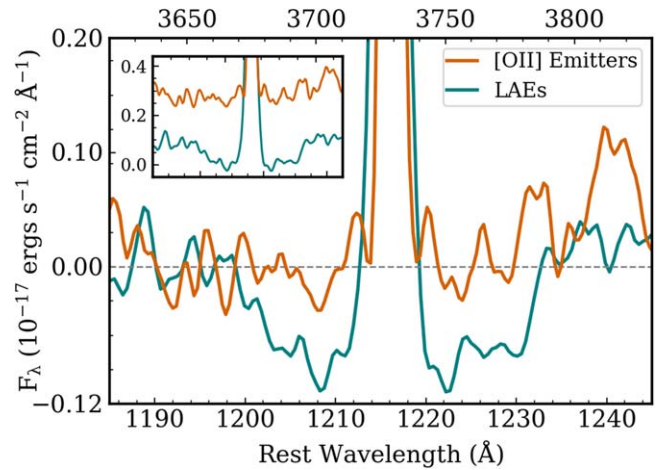


Figure 2. A stack of HETDEX LAEs alongside a stack of HETDEX $[\text{O II}]$ emitters. We compare emission lines of a similar brightness and/or equivalent width to ensure that the difference between them is intrinsic and not because of the properties of an emission-line detection. We chose the galaxies with g - or r -band counterpart magnitudes between 22 and 24, and line flux measurements $10\text{--}20 \times 10^{-17} \text{ erg s}^{-1} \text{ cm}^{-2}$. Each stack contains 100–250 spectra. Note that there are inherently few $[\text{O II}]$ and LAE detections that are similar in line brightness due to cosmological dimming. The inset displays the $[\text{O II}]$ and LAE stacks, and the main panel overlays the profiles (continuum subtracted). Both the inset and main panel are plotted on the same wavelength scale. While the stack of LAEs has absorption troughs, the stack of $[\text{O II}]$ emitters does not.

$\text{Ly}\alpha$ emission is present in HETDEX data (Lujan Niemeyer et al. 2022a, 2022b), troughs exist when using local sky subtraction *and* when using full-field sky subtraction. The full-field sky is measured from all of HETDEX's 34,944 fibers spread over a $21'$ field of view. This is far beyond the typical extent of $\text{Ly}\alpha$ emission (Wisotzki et al. 2018). Although there is a small amount of self-subtraction from $\text{Ly}\alpha$ halos in the local sky, the effect is minimal, and the depth of the troughs changes only by $\sim 5\%$ when using local versus full-field sky subtraction. Assuming significantly extended $\text{Ly}\alpha$ emission out to $\sim 1 \text{ cMpc}$ (Martin et al. 2023), the emission would have to be significantly brighter/broader at large radii where the sky is measured than on the LAE. If we instead stack spectra that have *not* been sky subtracted, the troughs around $\text{Ly}\alpha$ are still present.

Lastly, the $\text{Ly}\alpha$ line profile of Figure 1 could be due to an overwhelming number of $\text{Ly}\alpha$ false positives, each with the

shape shown in Figure 1. False positives arise when random noise is interpreted as a low-S/N emission line. As presented in Mentuch Cooper et al. (2023), the current false-positive rate for detections with an S/N of >5.5 is less than 15%. This rate is far too low to create the observed absorption troughs. Moreover, since there is no argument for the false positives consistently having the shape of spectral feature, we exclude the possibility that false positives are the cause of these troughs.

We conduct a number of additional tests to eliminate the possibility of a systematic issue within HETDEX’s calibration. These tests include stacking spectra of empty fibers, limiting the LAE sample to objects in specific amplifiers, and at varying S/N threshold for Ly α detections. As a basic test, we stack spectra from fibers chosen randomly spatially and in wavelength and, as expected, find no troughs. When stacking on LAEs, the troughs are consistent across amplifiers and are present with increasing line luminosity. The troughs, while not visible in an individual spectrum, appear in any random combination of ~ 100 or more LAEs.

The most convincing evidence that these absorption wings are not an artifact of data reduction and/or our stacking algorithm is that the troughs do *not* appear in the stacks of HETDEX [O II] emitters. [O II] $\lambda 3727$ is detected in HETDEX roughly as frequently as Ly α , and the spectrum of an [O II] galaxy is calibrated in exactly the same way as that of an LAE. Figure 2 compares a stack of HETDEX [O II] emitters to a stack of LAEs. For the sake of consistency, the spectra are chosen to have counterparts of a similar magnitude and similar line fluxes. Additionally, a possible continuum oversubtraction would be more evident in stacks of faint [O II] emitters. The stack of LAEs shows the absorption troughs, while the stack of [O II] emitters does not.

4.2. Ly α Troughs in Other Datasets

Two public data sets applicable to HETDEX are CLASSY (Berg et al. 2022) and MUSE-Wide (Bacon et al. 2010; Urrutia et al. 2019). The CLASSY data explore 45 nearby ($z < 0.2$) galaxies that are chosen to be similar to high-redshift LAEs. The MUSE-Wide sample overlaps HETDEX in redshift range and galaxy properties.

The CLASSY LAEs have Ly α luminosities $36.8 < \text{Log}(L_{\text{Ly}\alpha}) < 42.8$. After removing four galaxies from the CLASSY data set that have their Ly α profile contaminated by Ly α or O I from the Earth’s atmosphere, we have 41 galaxies that we divide visually into three subsamples: 19 with Ly α in absorption, four with Ly α emission sitting in an absorption well like those in HETDEX, and 22 with Ly α in emission. To compare to what we observe in HETDEX spectra, we rebin and convolve the CLASSY medium-resolution spectra ($\sim 0.03 \text{ \AA pixel}^{-1}$) to HETDEX resolution using a 2 \AA pixel^{-1} kernel, de-redshift the wavelengths using the galaxy’s systemic redshift according to Berg et al. (2022), fit a spline to their continua, and normalize to this fit.

Figure 3 depicts the three stacks of CLASSY spectra. The leftmost panel shows the 19 galaxies with Ly α absorption, the middle panel depicts the four CLASSY spectra with Ly α emission and absorption, and the rightmost panel represents the 22 galaxies with Ly α emission. A number of additional absorption and emission features are present, such as Si II $\lambda\lambda 1090, 1093$ and N V $\lambda\lambda 1238, 1242$. The shape of the middle profile differs from the HETDEX stack, as it more

closely follows a typical Voigt profile, rather than the “boxy” troughs seen in Figure 1. For these particular CLASSY profiles, Hu et al. (2023) reports that they are indicative of an inhomogeneous ISM with outflows and can be modeled by splitting the H I covering factor between low- and high-density channels. Additionally, while several Ly α absorption profiles in CLASSY are saturated, none are negative.

Galaxies in the MUSE-Wide survey have redshifts at $2.9 < z < 6.3$. To compare to typical HETDEX LAEs, we first select the galaxies with $z \lesssim 4.3$, then we further select galaxies with Ly α line fluxes in the fainter 55% of the MUSE sample’s flux distribution ($< \sim 3 \times 10^{-17} \text{ erg s}^{-1} \text{ cm}^{-2} \text{ \AA}^{-1}$). Both cut-offs are chosen roughly to reproduce the HETDEX Ly α flux distribution while keeping ~ 200 individual spectra in each stack. We de-redshift the wavelengths of each spectra using the reported redshift from MUSE, but keep the flux densities in the observed frame. The stack of 169 MUSE-Wide galaxies is shown in Figure 4. As with HETDEX, there are absorption troughs around Ly α emission, and, interestingly, the troughs are negative. We did not apply the corrections to convert the fluxes to the rest frame, nor did we continuum subtract.

The troughs seen in the CLASSY stack are consistent with absorption from the ISM. Those seen in MUSE-Wide are similar to what we observe in HETDEX, both in their negative flux values and “boxy” shape. These types of troughs are the focus of this paper. The physical origin of the troughs will be discussed further in Section 5.

4.3. Ly α Troughs in HETDEX

With hundreds of thousands of available LAE spectra, we stack according to host-galaxy properties to investigate if the troughs change with the subsample. We first determine whether the absorption troughs are unique to LAEs that are significantly brighter or fainter in the continuum than the typical HETDEX LAE. About 25,000 HETDEX LAEs have confirmed counterparts via ELiXer cross-matching to various catalogs in the r and/or g band. We restrict this sample to the $2.4 < z < 2.6$ redshift range to mitigate any redshift evolution and stack galaxies according to apparent magnitude in either band. The wavelengths of the spectra are shifted to the rest frame, while the fluxes remain in the observed frame, as any multiplicative correction for cosmological dimming will deepen the artificially negative troughs. The stacks of these galaxies as well as those without a counterpart are displayed in the left panel of Figure 5. The troughs are present in LAEs with and without counterparts, and are not unique to galaxies of a certain magnitude. However, whether or not the troughs are negative does change, likely because our oversubtraction of sky flux does not push the troughs negative in LAEs with more underlying continuum flux.

As a second experiment, we again confine our analysis to LAEs in the redshift range $2.4 < z < 2.6$, but we now fix the g and r continuum magnitudes ($24 < m < 25$), while subdividing the sample by Ly α line luminosity. The troughs in the right panel of Figure 5 are not negative due to the bright continuum level of this sample. The stack of galaxies with the faintest Ly α emission has the strongest troughs, while the stacks of galaxies with more Ly α emission have slightly weaker troughs. In the highest-luminosity bin, the redward trough has been filled in by Ly α emission. This effect resembles the asymmetry of the troughs seen in Figure 1, as slightly higher-S/N spectra (S/N > 5.5) contribute to the stack. This trend with luminosity

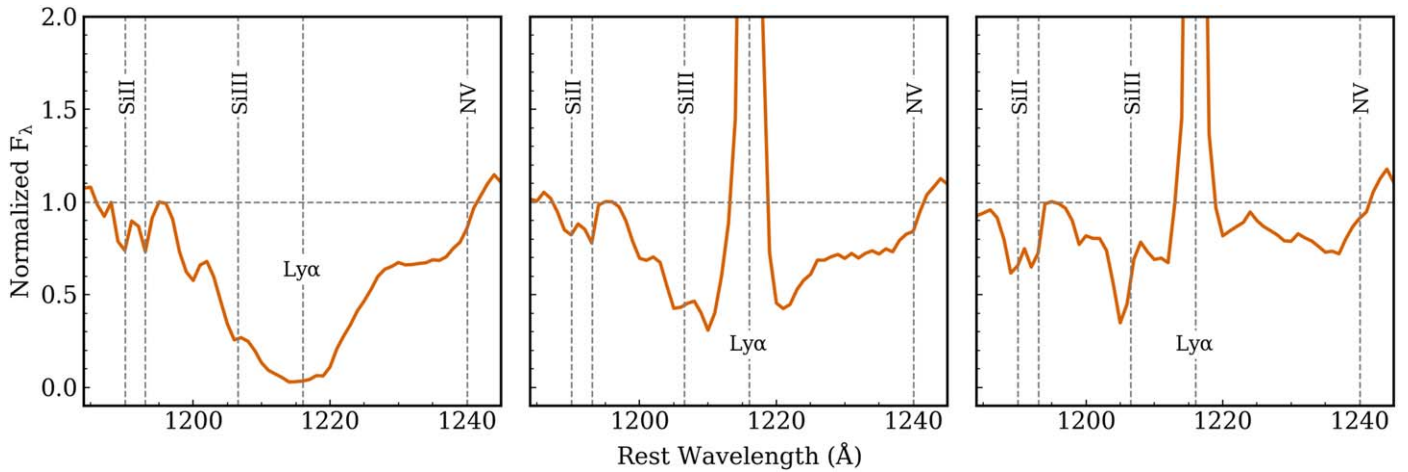


Figure 3. Spectral stacks of the galaxies in the CLASSY sample normalized to their continua. Left panel: a stack of the 19 CLASSY galaxies that exhibit pure $\text{Ly}\alpha$ absorption. Various other absorption features can be seen, such as N V and Si II. Middle panel: a stack of four CLASSY galaxies, each individually appearing to have $\text{Ly}\alpha$ emission sitting in an absorption trough. The absorption redward of the $\text{Ly}\alpha$ emission appears slightly wider than that observed in HETDEX. Right panel: a stack of all 22 CLASSY galaxies that have $\text{Ly}\alpha$ emission. There is absorption from the N V P Cygni profile near $\text{Ly}\alpha$, but an obvious $\text{Ly}\alpha$ absorption profile is not apparent.

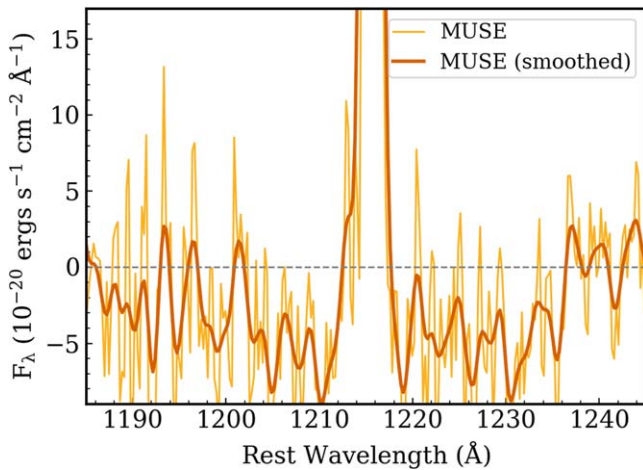


Figure 4. A stack of 169 MUSE-Wide LAE spectra selected at $2.9 < z < 4.3$ that have comparatively lower $\text{Ly}\alpha$ line fluxes. The unsmoothed stacked spectrum is indicated in yellow, and the spectrum smoothed by a Gaussian kernel of 3 pixels is shown in orange. As with HETDEX stacks, we observe $\text{Ly}\alpha$ absorption troughs on either side of the emission, and we also find that these troughs are negative. These troughs more closely resemble the “boxy” profiles we see in the HETDEX stack.

lends itself to the idea that these troughs do not arise due to instrumental/electronics issues, as more flux from the emission line would create deeper troughs.

While we currently have the capabilities to stack as a function of redshift, we reserve this analysis for a future paper. Until we apply a physical model, the depths of the troughs will be artificially enhanced by the corrections to the rest frame. For the remainder of this paper, we focus on developing a physical interpretation of the negative troughs.

5. Physical Model of $\text{Ly}\alpha$ Troughs

A physical model of the absorption troughs must explain three primary observables: the depth of the absorption troughs, the width of the troughs, and the fact that they go negative with our sky subtraction. To begin investigating the physical origins of the $\text{Ly}\alpha$ troughs, we note their similarity to DLAs.

In DLAs, background light from a bright source such as a quasar is considerably absorbed at the $\text{Ly}\alpha$ transition by hydrogen from intervening galaxies or protogalaxies both in the core of $\text{Ly}\alpha$ and in the damped wings of the line (Wolfe et al. 1995). The high HI column density ($N(\text{H I}) \geq 10^{20} \text{ cm}^{-2}$) and frequency of these absorbers account for a significant fraction of the neutral hydrogen content in the Universe between $0 < z < 5$ (Storrie-Lombardi & Wolfe 2000).

DLA systems that also have $\text{Ly}\alpha$ emission from the foreground galaxy (such as the one presented in Figure 1 of Møller et al. 2004) are similar to the profile shapes we see in stacks of HETDEX LAEs. While it is clear that these troughs are not absorption of a bright individual background galaxy such as a quasar, we propose a solution using a similar geometry. In the model described below, the source of the light in the background of the LAEs is dependent on the density of the nearby galaxy population.

5.1. Background Light

The integrated light from galaxies behind the LAEs provides a spectrum of background radiation. Theoretically, there has been significant effort in modeling the radiative transfer of UV emission from AGNs and star-forming galaxies through the IGM (e.g., Miralda-Escude & Ostriker 1990; Giroux & Shapiro 1996; Haardt & Madau 1996; Faucher-Giguère et al. 2009; Haardt & Madau 2012), which produces an evolving UV background.

Observationally, redshifted photons from all sources throughout cosmic history have been observed across the electromagnetic spectrum as extragalactic background light (Lauer et al. 2022). These studies generally measure a background light that is representative of an average over the full sky. In our case, we require a more local background spectrum, although the spectrum should be similar in shape, since it is due to stars in the background galaxies. The flux of the background, however, will vary with the density of nearby galaxies.

LAE at $z \sim 3$ trace the large-scale clustering of galaxies, with a linear bias likely in the range between ~ 1.4 and ~ 2.0 (Gawiser et al. 2007; Guaita et al. 2010; Kusakabe et al. 2019).

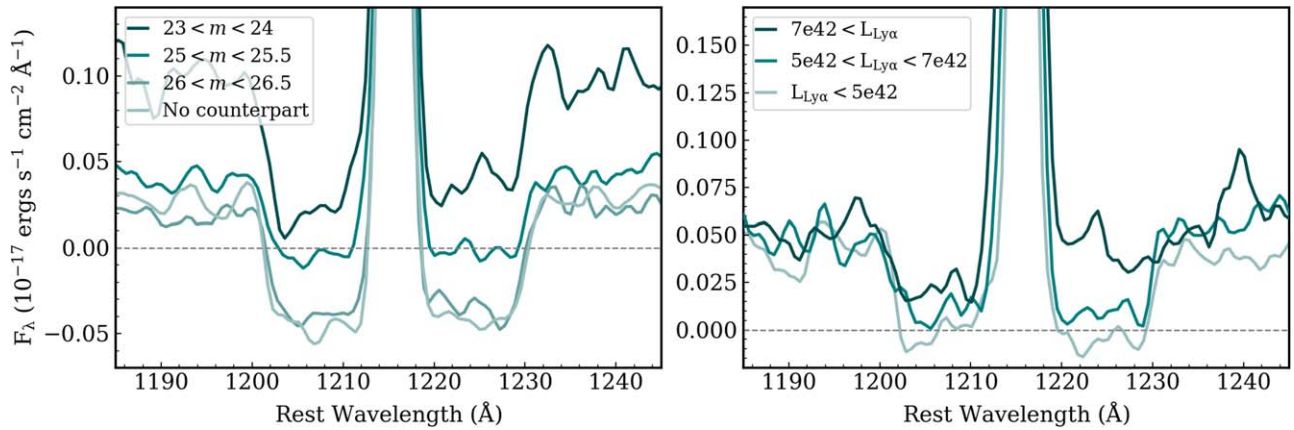


Figure 5. Left panel: stacks of HETDEX LAEs in counterpart magnitude bins. We restricted these subsamples to have $z \sim 2.5$ and $5 < S/N < 8$. The troughs themselves are present in each stack, although are not negative in stacks of brighter LAEs. This behavior is likely due to higher continuum levels. Right panel: stacks of HETDEX LAEs in three $\text{Ly}\alpha$ luminosity bins. These galaxies are selected to have counterpart magnitudes between 24 and 25 and $z \sim 2.5$. The strongest $\text{Ly}\alpha$ absorption troughs appear in the stacks of galaxies with the faintest $\text{Ly}\alpha$ emission. In the highest-luminosity bin, the red trough is entirely filled in by $\text{Ly}\alpha$ in emission. For both panels, there are roughly 200–1000 spectra contributing to the stacks.

Since the VIRUS fiber diameter and median HETDEX image quality are both moderately large ($1''.5$ and $1''.7$, respectively), the individual spectra contain contributions well into the halos of $z \sim 2$ – 3 LAEs. Therefore, every HETDEX observation of an LAE must also contain diffuse flux from background sources both nearby and distant, as well as absorption at $\text{Ly}\alpha$ by gas in the halo. Averaging over tens of thousands of LAEs will account for galaxies of all magnitudes, including bright neighbors. The absorption troughs only become significant when stacking, since the intensity of the background spectrum in the observed frame is significantly fainter than the typical noise in a single-fiber spectrum. In this picture, the troughs deepen with increasing density of background galaxies. Thus, the absorption around $\text{Ly}\alpha$ should be strongest in overdense fields. We can test this hypothesis by examining the behavior of the $\text{Ly}\alpha$ emission versus environment. To do this, we start by determining the local galaxy luminosity function for every HETDEX pointing.

Each individual $21'$ field for HETDEX contains anywhere from ~ 100 to ~ 400 LAEs. These LAEs have redshifts from $1.88 < z < 3.52$; we can generate a luminosity function from each field with this pencil-beam geometry. We can then normalize these functions to the luminosity function formed from all $\sim 800,000$ LAEs contained in the 3993 fields of HDR3 (K. Gebhardt et al. 2024, in preparation; D. Jeong et al. 2024, in preparation) to obtain a rough estimate of the relative galaxy density along each line of sight. Although we would prefer to use an estimate of environment that uses the galaxy density surrounding each LAE, rather than one based on a line-of-sight summation, the integrated approach is the best that can be done with the present data.

Using these luminosity function normalizations (LF_{norm}), we define three environments: overdense ($1.6 < LF_{\text{norm}} < 1.61$), underdense ($0.3 < LF_{\text{norm}} < 0.4$), and void ($0 < LF_{\text{norm}} < 0.28$) regions. The limits and bin widths are chosen only to ensure sufficient spectra to stack, as there are naturally more galaxies in overdense fields. The stacked spectra of the galaxies within each bin are presented in Figure 6. The troughs are barely visible in very underdense regions and become more significant and negative with increasing field density. While more robust density calculations are needed for further analyses, the

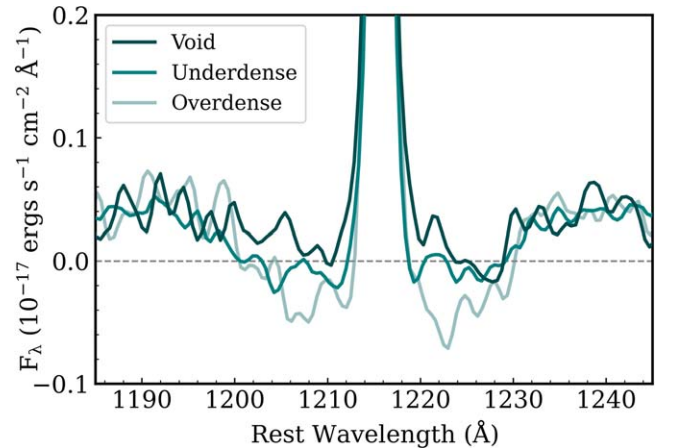


Figure 6. Stacks of galaxies that reside in over-, under-, and very underdense fields using the luminosity function normalization as a proxy for density. The widths of the bins are chosen to have ~ 80 – 200 contributing LAEs, with a similar number of spectra contributing to each stack. The troughs are weakest in very underdense fields and strongest in overdense fields. The troughs in the overdense stack are the most negative, despite all three bins having similar continuum levels.

observed trend is consistent with our proposed background light absorption scenario.

5.2. Oversubtraction of Sky

Negative troughs are consistent with the physical interpretation that typical LAEs absorb background light produced by nearby galaxies. The negative troughs arise because the flux at the wavelength of $\text{Ly}\alpha$ is removed from a spectrum twice: first physically by an LAE and then again during the sky-subtraction procedure.

When the background photons at the resonance wavelength of $\text{Ly}\alpha$ are scattered by HI and absorbed by dust in a galaxy's halo, the contribution of the background at $\text{Ly}\alpha$ is removed, creating the troughs like those in our stacked fiber spectra. When applying the sky subtraction (see Section 3.1), we assume that the background sky is the same in the nearby fibers as it is in the fiber centered on the LAE. Since this assumption is *not* correct due to the HI absorption, we oversubtract at $\text{Ly}\alpha$. As a result, the troughs in the subtracted spectrum are pushed

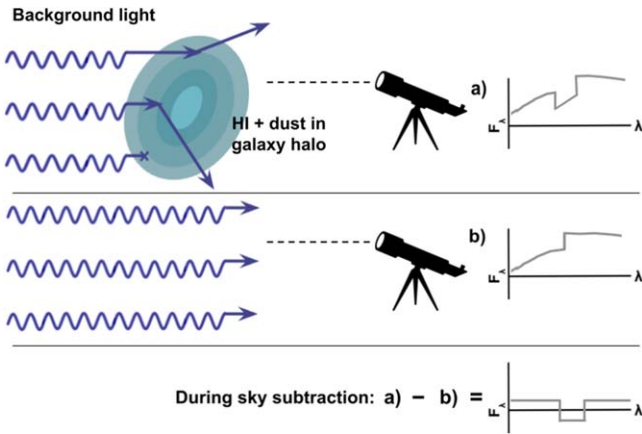


Figure 7. A simplified, 1D graphic depicting our proposed interpretation of the negative $\text{Ly}\alpha$ troughs. In (a), background UV light is absorbed at the wavelength of $\text{Ly}\alpha$ by H I gas in the halo of the LAE, creating an absorption well in the combined spectrum. The $\text{Ly}\alpha$ emission from the foreground LAE is not shown for clarity. In (b), the spectrum observed off source (empty sky) includes this UV background *without* the $\text{Ly}\alpha$ absorption. The shape of the background spectrum is as modeled by Haardt & Madau (2012), while the shape of the absorption and LAE continuum are simple representations. During HETDEX’s sky subtraction, (b) is subtracted from (a), creating the negative absorption seen in the bottom panel.

negative depending on the object’s continuum level. The stack of MUSE spectra in Figure 4 shows similar negative troughs; whether or not they are due to the same physical interpretation depends on the MUSE sky-subtraction procedure.

Figure 7 depicts a graphic of the oversubtraction process. In this figure, the top panel presents the full, on-target spectrum, the middle panel shows the spectrum off target (i.e., our measurement of the sky), and the bottom panel displays the sky-subtracted spectrum. Since we assume that the off-source sky is the same as the on-source sky, we oversubtract at $\text{Ly}\alpha$ due to the absorption by H I in the halo of the LAE.

Because the background flux is faint, the oversubtraction at the wavelength of $\text{Ly}\alpha$ on a per-fiber basis for an individual LAE is negligible. By stacking the spectra of hundreds to thousands of LAEs, the negative troughs become significant. In essence, a slight oversubtraction in the HETDEX data is indicative of local density enhancements and gas present in LAE halos.

5.3. $\text{Ly}\alpha$ Profile Modeling

To further investigate our interpretation of the $\text{Ly}\alpha$ absorption troughs, we create a phenomenological model of the $\text{Ly}\alpha$ profile. We use Radiative SCattering in Astrophysical Simulations (RASCAS; Michel-Dansac et al. 2020) to model the proposed background absorption scenario, with the goal of reproducing the observed absorption troughs in HETDEX.

Using the HPSC-1 stack shown in Figure 1, we attempt to “undo” the oversubtraction caused by HETDEX sky subtraction. To each sky-subtracted, observed-frame LAE spectrum, we add a spectrum with the shape modeled by Haardt & Madau (2012) for the given redshift shifted in wavelength space to the observed frame. Although the spectrum from Haardt & Madau (2012) is integrated from the redshift of the LAE to infinity and does not account for local density variations, the source of the radiation is similar.

However, for each individual LAE in the stacked spectrum, we do not know the background flux due to the density variations. Since our goal is to use this model to explain the oversubtraction, we apply the Haardt & Madau (2012) spectrum scaled such that the depths of absorption troughs in the stacked spectrum are no longer negative. This scaling is likely not correct due to the unaccounted for contribution of the underlying continuum of the LAEs.

This procedure creates the average combined background and LAE spectrum for HPSC-1 (see the black line in Figure 9, plotted in normalized units). The troughs are no longer negative and the asymmetry of the profile has been enhanced due to the addition of the scaled, asymmetric (Haardt & Madau 2012) background spectrum. This procedure also generates an average background spectrum, which is used as input to the simulation described below. We aim only to reproduce the troughs with physical geometry. Given our assumptions in this model, we do not attempt to quantify the intensity of the background or properties of the gas at this time.

RASCAS is used to build a simple idealized model of our proposed scenario, with parameters chosen to reproduce the troughs seen in the HPSC-1 stack. We simulate a source of $\text{Ly}\alpha$ photons at systemic velocity surrounded by a shell of H I, with column density $N(\text{H I}) = 10^{18} \text{ cm}^{-2}$ and a small density of dust ($n_{\text{dust}} = 0.01 \text{ cm}^{-3}$) per cell at the systemic velocity of the LAE. Note, because we stack using $\text{Ly}\alpha$ -based redshifts, the $\text{Ly}\alpha$ emission is centered at 0 km s^{-1} . This $\text{Ly}\alpha$ source is partially ($\sim 30\%$) embedded in a screen of H I ($N(\text{H I}) = 10^{19.5} \text{ cm}^{-2}$) with $n_{\text{dust}} = 0.005 \text{ cm}^{-3}$. To determine parameters for the H I screen, we fit a single Voigt profile to the stack’s absorption well (see the inset plot of Figure 9). This fit yields a velocity offset of -100 km s^{-1} (blueward of the $\text{Ly}\alpha$ emission) and a Doppler broadening parameter, b , of 1050 km s^{-1} , which we adopt for the screen. We then model a continuum source with the spectrum and intensity of the average stacked background described above, also at systemic velocity. This continuum is placed behind the H I screen. A graphic of this geometry is depicted in Figure 8.

With this configuration, we create 35,000 photon packets emitted at 0 km s^{-1} to sample a Gaussian $\text{Ly}\alpha$ profile and 15,000 to sample a background spectrum. We propagate all photons through the geometry described above with RASCAS. Each time the photon enters a cell, the optical depth of the H I and dust in the cell is computed, and then the probability that this photon is scattered by H I or absorbed by dust is calculated. If the photon is scattered, it is assigned a random direction for reemission with a new calculated frequency. This procedure is repeated through the grid for each photon. The final profile includes all the photons that escape in a randomly chosen viewing direction.

In this model, the background photons are scattered and absorbed by the dense screen, producing the broad absorption well. Because the $\text{Ly}\alpha$ source is only partially embedded in the screen, the $\text{Ly}\alpha$ photons scatter in the less dense shell and a large fraction manage to escape along the line of sight, producing the observed $\text{Ly}\alpha$ emission. The geometric picture that the LAE is asymmetrically embedded in the H I screen makes sense, as LAEs obscured by a sufficient amount of H I (even with a low density of dust) would not be detected in emission. Thus, we are likely observationally biased toward LAEs with less material in the immediate foreground. In this case, there are also likely fewer galaxies in the foreground of

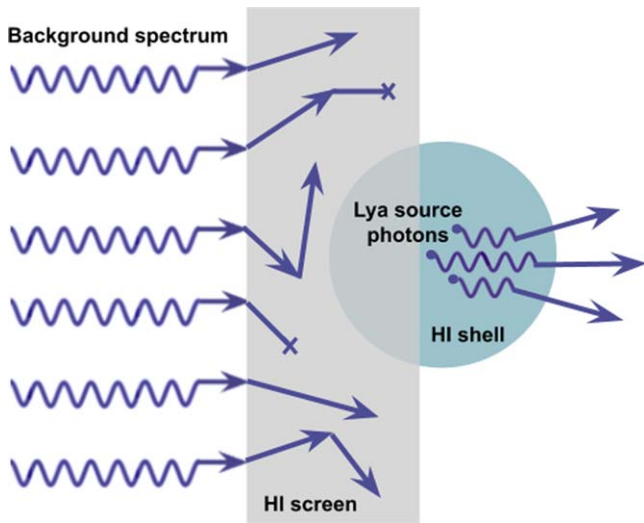


Figure 8. A graphic of the geometry used in modeling our proposed absorption scenario (note that this is an oversimplification of the physical model we suggest and serves only to illustrate the basic geometry). We place a continuum source that represents the average stacked “background spectrum” behind a screen of H I. We then model a foreground “LAE” as a source of Ly α photons surrounded by a less dense shell of H I and partially embed it in the screen. The background photons are scattered/absorbed by the H I screen, producing the absorption well. The foreground Ly α source photons scatter in the less dense shell and escape along the line of sight for observation. The degree to which the “LAE” is embedded in the screen affects only the shape of the Ly α emission component, which we set to reproduce the emission observed in our stacks. The overall profile is then the combination of the background absorption well and the foreground Ly α emission.

the LAE than in the background, creating the local, anisotropic background consistent with this model. The resulting profile is the sum of the foreground LAE and absorption of the local background.

The red line in Figure 9 represents the spectrum generated by the parameters described above and is scaled in relative units. The inset panel depicts the profile of only the background and H I screen component. This creates an underlying saturated absorption well, without the contribution of the Ly α emission. Adding the embedded Ly α photon source produces the combined emission and absorption profile. This model can produce symmetric, broad, and boxy troughs similar to those observed in HETDEX stacks. The red trough of the stack is shallower than in the model, i.e., similar to the luminosity trend in Figure 5. It is possible that this asymmetry in the troughs is influenced by high-Ly α luminosity spectra contributing to the HPSC-1 stack, although more complex models that include stellar continua are needed to investigate this further. Changing the density of dust and the degree to which the Ly α -emitting region is embedded in the H I screen changes the shape of the Ly α emission component, which alters the overall combined profile. We reserve the fine-tuning of these parameters for a future paper.

If we assume the Ly α emission of the HPSC-1 stack is redshifted from systemic by ~ 250 km s $^{-1}$ (Davis et al. 2023a), the absorbing gas of the fit model (-100 km s $^{-1}$) is redshifted from the systemic velocity by ~ 150 km s $^{-1}$. While there are several combinations of b and $N(\text{H I})$ that produce similar profiles, in order to reproduce the broad and boxy troughs seen in HETDEX, b must be large. If we instead restrict $b < 200$ km s $^{-1}$ to reflect typical conditions of the ISM, the modeled profile more closely resembles the stack of the four

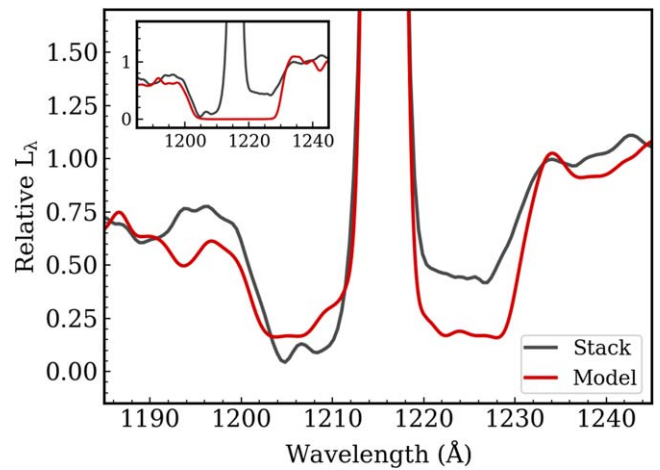


Figure 9. The Ly α profile produced by our simulation of a background flux absorption scenario. The modeled profile is indicated in red and the HPSC-1 combined spectrum we fit to is plotted in gray. The upper-left inset displays the profile fit to the absorption only. While the model does not simulate the continuum of the LAE and adopts a simple screen geometry for H I gas and dust, it is able to reproduce a profile resembling the absorption troughs around Ly α .

CLASSY galaxies with Ly α absorption and emission (see the middle panel of Figure 3). The Ly α profiles in these CLASSY galaxies have been previously fitted in this manner (Hu et al. 2023).

The need for a much larger Doppler parameter to replicate the absorption troughs in the HETDEX stacks may indicate that the absorbing gas is not within the ISM (though some amount of LAE continuum absorption by the ISM likely contributes to the overall profile). The HPSC-1 stack is made using LAEs from different redshifts; thus any evolution of the troughs will be artificially smeared and affect the profile.

We can empirically determine the absorption profile by subtracting the HPSC-1 stack from our expectation for Ly α using the CLASSY stack (see the right panel of Figure 3). The continuum-normalized HPSC-1 stacks are displayed in the top panel of Figure 10, and the subtraction of the two is given in the bottom panel, masking the central Ly α emission. The HPSC-1 stack has been shifted by 250 km s $^{-1}$ to account for the Ly α velocity offset from systemic. Effectively, the shape of this subtracted profile is representative of the typical absorption of background flux by H I in the halo of LAEs.

6. Summary

The unprecedented number of LAE spectra in HETDEX provides an opportunity to explore the production and radiative transfer of Ly α in the $1.9 < z < 3.5$ epoch of the Universe. While an individual LAE spectrum lacks sufficient S/N for in-depth measurements of the Ly α profile or continuum level, a stack of LAEs can provide far more detail and reach flux limits impossible to otherwise attain.

In this paper, we explored spectral stacks of up to 50,000 LAEs. Such data not only enable investigations of weak absorption features in the continua of these objects, but also the detailed analysis of the Ly α line profiles. One of the main obvious features consistent across these stacks is the deep absorption around the wavelength of Ly α . While these troughs reach flux density levels below zero, we argue that their

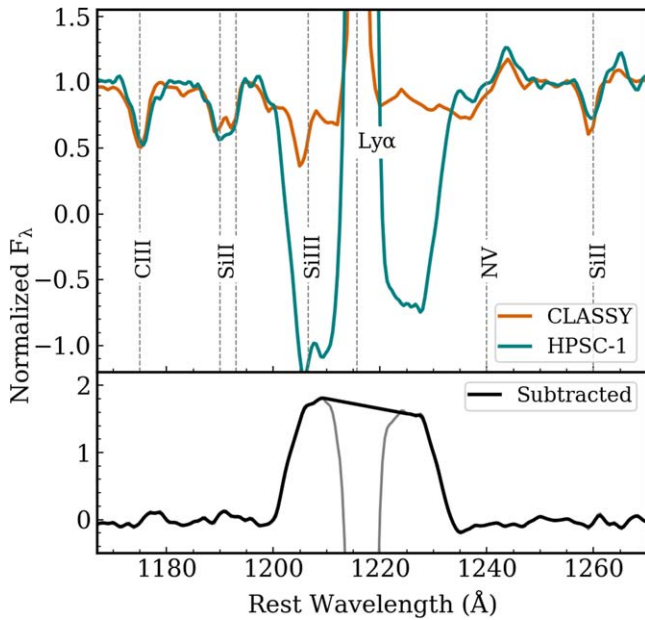


Figure 10. Upper panel: the HPSC-1 stack compared to the stack of CLASSY LAEs convolved to the spectral resolution of VIRUS (see the rightmost panel of Figure 3). Both stacks have been normalized to their continuum. The HPSC-1 stack has also been shifted by 250 km s^{-1} to account for the $\text{Ly}\alpha$ velocity offset from systemic. Lower panel: the normalized HPSC-1 stack subtracted from the normalized CLASSY stack, with the $\text{Ly}\alpha$ emission masked out. In the background absorption scenario, this profile reflects the absorption of the integrated flux from background sources by H I in the LAE halo.

existence is not an artifact of the data, but are a real feature of LAE spectra.

We propose a model wherein flux from nearby background sources is absorbed by the H I gas around the LAE, in a geometry similar to that of DLAs. This flux is over-subtracted around the wavelength of $\text{Ly}\alpha$ during our sky-subtraction procedure, creating negative troughs, whose depths depend on the local density enhancements. We use field number counts as a proxy for the density around the LAE, and stack galaxies in over- and underdense fields. We find that the strengths of the troughs increase with density. A simple radiative-transfer simulation created to model this geometry is able to produce troughs similar to those seen in HETDEX stacks.

HETDEX will eventually have more than one million LAE spectra from $1.88 < z < 3.52$, and we will be able to combine spectra in various ways. Of particular interest in future work is the evolution of the absorption troughs with redshift and environment. To explore the spatial distribution of background absorption, we plan to stack spectra in annuli around the LAEs as well as between LAE pairs. With more in-depth simulations, we aim to determine the intensity of the LAEs' local background and to quantify the properties and evolution of the absorbing gas.

Acknowledgments

HETDEX is led by the University of Texas at Austin McDonald Observatory and Department of Astronomy with participation from the Ludwig-Maximilians-Universität München, Max-Planck-Institut für Extraterrestrische Physik (MPE), Leibniz-Institut für Astrophysik Potsdam (AIP), Texas A&M University, The Pennsylvania State University, Institut für Astrophysik Göttingen, the University of Oxford, Max-Planck-Institut für Astrophysik (MPA), The University of

Tokyo, and Missouri University of Science and Technology. In addition to Institutional support, HETDEX is funded by the National Science Foundation (grant AST-0926815), the State of Texas, the US Air Force (grant No. AFRL FA9451-04-2-0355), and generous support from private individuals and foundations.

Observations were obtained with the Hobby–Eberly Telescope (HET), which is a joint project of the University of Texas at Austin, the Pennsylvania State University, Ludwig-Maximilians-Universität München, and Georg-August-Universität Göttingen. The HET is named in honor of its principal benefactors, William P. Hobby and Robert E. Eberly.

VIRUS is a joint project of the University of Texas at Austin, Leibniz-Institut für Astrophysik Potsdam (AIP), Texas A&M University (TAMU), Max-Planck-Institut für Extraterrestrische Physik (MPE), Ludwig-Maximilians-Universität Muenchen, Pennsylvania State University, Institut für Astrophysik Göttingen, the University of Oxford, and the Max-Planck-Institut für Astrophysik (MPA). In addition to institutional support, VIRUS was partially funded by the National Science Foundation, the State of Texas, and generous support from private individuals and foundations.

The authors acknowledge the Texas Advanced Computing Center (TACC) at The University of Texas at Austin for providing high-performance computing, visualization, and storage resources that have contributed to the research results reported within this paper (<http://www.tacc.utexas.edu>).

The Institute for Gravitation and the Cosmos is supported by the Eberly College of Science and the Office of the Senior Vice President for Research at the Pennsylvania State University.










K.G. acknowledges support from NSF-2008793. E.G. acknowledges support from NSF grant AST-2206222. A.S.L. acknowledges support from Swiss National Science Foundation. H.K. and S.S. acknowledge support for this work from NSF-2219212. E.K. and S.S. are supported in part by the World Premier International Research Center Initiative (WPI Initiative), MEXT, Japan.

Facility: HET.

Software: Astropy (AstroPy Collaboration et al. 2018), NumPy (Harris et al. 2020), SciPy (Virtanen et al. 2020), Matplotlib (Hunter 2007), EliXer (Davis et al. 2023b).

ORCID iDs

Laurel H. Weiss <https://orcid.org/0000-0002-4974-1243>
Dustin Davis <https://orcid.org/0000-0002-8925-9769>
Karl Gebhardt <https://orcid.org/0000-0002-8433-8185>
Simon Gazagnes <https://orcid.org/0000-0002-5659-4974>
Mahan Mirza Khanlari <https://orcid.org/0009-0003-1893-9526>
Erin Mentuch Cooper <https://orcid.org/0000-0002-2307-0146>
John Chisholm <https://orcid.org/0000-0002-0302-2577>
Danielle Berg <https://orcid.org/0000-0002-4153-053X>
William P. Bowman <https://orcid.org/0000-0003-4381-5245>
Chris Byrohl <https://orcid.org/0000-0002-0885-8090>
Robin Ciardullo <https://orcid.org/0000-0002-1328-0211>
Maximilian Fabricius <https://orcid.org/0000-0002-7025-6058>
Daniel Farrow <https://orcid.org/0000-0003-2575-0652>
Caryl Gronwall <https://orcid.org/0000-0001-6842-2371>
Gary J. Hill <https://orcid.org/0000-0001-6717-7685>

Lindsay R. House  <https://orcid.org/0000-0002-1496-6514>
 Donghui Jeong  <https://orcid.org/0000-0002-8434-979X>
 Hasti Khoraminezhad  <https://orcid.org/0000-0001-5610-4405>
 Wolfram Kollatschny  <https://orcid.org/0000-0002-0417-1494>
 Eiichiro Komatsu  <https://orcid.org/0000-0002-0136-2404>
 Maja Lujan Niemeyer  <https://orcid.org/0000-0002-6907-8370>
 Shun Saito  <https://orcid.org/0000-0002-6186-5476>
 Donald P. Schneider  <https://orcid.org/0000-0001-7240-7449>
 Gregory R. Zeimann  <https://orcid.org/0000-0003-2307-0629>

References

- Andrews, D. F., Bickel, P. J., Hampel, F. R., et al. 1972, *Robust Estimates of Location: Survey and Advances* (Princeton, NJ: Princeton Univ. Press)
- AstroPy Collaboration, Price-Whelan, A. M., SipHocz, B. M., et al. 2018, *AJ*, **156**, 123
- Bacon, R., Adjali, L., Anwand, H., et al. 2010, *Proc. SPIE*, **7735**, 773508
- Beers, T. C., Flynn, K., & Gebhardt, K. 1990, *AJ*, **100**, 32
- Berg, D. A., James, B. L., King, T., et al. 2022, *ApJS*, **261**, 31
- Chung, A. S., Dijkstra, M., Ciardi, B., Kakiichi, K., & Naab, T. 2019, *MNRAS*, **484**, 2420
- Cowie, L. L., Barger, A. J., & Hu, E. M. 2010, *ApJ*, **711**, 928
- Davis, D., Gebhardt, K., Cooper, E. M., et al. 2023a, *ApJ*, **954**, 209
- Davis, D., Gebhardt, K., Cooper, E. M., et al. 2023b, *ApJ*, **946**, 86
- Davis, D., Gebhardt, K., Mentuch Cooper, E., et al. 2021, *ApJ*, **920**, 122
- Dijkstra, M., & Kramer, R. 2012, *MNRAS*, **424**, 1672
- Erb, D. K., Steidel, C. C., Trainor, R. F., et al. 2014, *ApJ*, **795**, 33
- Faucher-Giguère, C.-A., Lidz, A., Zaldarriaga, M., & Hernquist, L. 2009, *ApJ*, **703**, 1416
- Finkelstein, S. L., Rhoads, J. E., Malhotra, S., Grogin, N., & Wang, J. 2008, *ApJ*, **678**, 655
- Gawiser, E., Francke, H., Lai, K., et al. 2007, *ApJ*, **671**, 278
- Gebhardt, K., Mentuch Cooper, E., Ciardullo, R., et al. 2021, *ApJ*, **923**, 217
- Giroux, M. L., & Shapiro, P. R. 1996, *ApJS*, **102**, 191
- Greisen, E. W., Calabretta, M. R., Valdes, F. G., & Allen, S. L. 2006, *A&A*, **446**, 747
- Guaita, L., Gawiser, E., Padilla, N., et al. 2010, *ApJ*, **714**, 255
- Gunn, J. E., & Peterson, B. A. 1965, *ApJ*, **142**, 1633
- Haardt, F., & Madau, P. 1996, *ApJ*, **461**, 20
- Haardt, F., & Madau, P. 2012, *ApJ*, **746**, 125
- Hansen, M., & Oh, S. P. 2006, *MNRAS*, **367**, 979
- Harris, C. R., Millman, K. J., van der Walt, S. J., et al. 2020, *Natur*, **585**, 357
- Hill, G. J., Kelz, A., Lee, H., et al. 2018, *Proc. SPIE*, **10702**, 107021K
- Hill, G. J., Lee, H., MacQueen, P. J., et al. 2021, *AJ*, **162**, 298
- Hu, E. M., Kim, T.-S., Cowie, L. L., Songaila, A., & Rauch, M. 1995, *AJ*, **110**, 1526
- Hu, W., Martin, C. L., Gronke, M., et al. 2023, *ApJ*, **956**, 39
- Hunter, J. D. 2007, *CSE*, **9**, 90
- Jaskot, A. E., & Oey, M. S. 2014, *ApJL*, **791**, L19
- Kunth, D., Mas-Hesse, J. M., Terlevich, E., et al. 1998, *A&A*, **334**, 11
- Kusakabe, H., Shimasaku, K., Momose, R., et al. 2019, *PASJ*, **71**, 55
- Lauer, T. R., Postman, M., Spencer, J. R., et al. 2022, *ApJL*, **927**, L8
- Liu, C., Gebhardt, K., Kollatschny, W., et al. 2022, *ApJ*, **940**, 40
- Lujan Niemeyer, M., Bowman, W. P., Ciardullo, R., et al. 2022a, *ApJL*, **934**, L26
- Lujan Niemeyer, M., Komatsu, E., Byrohl, C., et al. 2022b, *ApJ*, **929**, 90
- Lynds, R. 1971, *ApJL*, **164**, L73
- Martin, D. C., Darvish, B., Lin, Z., et al. 2023, *NatAs*, **7**, 1390
- Matsuda, Y., Yamada, T., Hayashino, T., et al. 2012, *MNRAS*, **425**, 878
- Mentuch Cooper, E., Gebhardt, K., Davis, D., et al. 2023, *ApJ*, **943**, 177
- Michel-Dansac, L., Blaizot, J., Garel, T., et al. 2020, *A&A*, **635**, A154
- Miralda-Escude, J., & Ostriker, J. P. 1990, *ApJ*, **350**, 1
- Møller, P., Fynbo, J. P. U., & Fall, S. M. 2004, *A&A*, **422**, L33
- Neufeld, D. A. 1991, *ApJL*, **370**, L85
- Oke, J. B., & Gunn, J. E. 1983, *ApJ*, **266**, 713
- Ouchi, M., Ono, Y., & Shibuya, T. 2020, *ARA&A*, **58**, 617
- Ouchi, M., Shimasaku, K., Akiyama, M., et al. 2008, *ApJS*, **176**, 301
- Park, H., Jung, I., Song, H., et al. 2021, *ApJ*, **922**, 263
- Partridge, R. B., & Peebles, P. J. E. 1967, *ApJ*, **147**, 868
- Planck Collaboration I 2020, *A&A*, **641**, A1
- Ramsey, L. W., Adams, M. T., Barnes, T. G., et al. 1998, *Proc. SPIE*, **3352**, 34
- Rivera-Thorsen, T. E., Hayes, M., Östlin, G., et al. 2015, *ApJ*, **805**, 14
- Scarlata, C., Colbert, J., Teplitz, H. I., et al. 2009, *ApJL*, **704**, L98
- Schaerer, D., Hayes, M., Verhamme, A., & Teyssier, R. 2011, *A&A*, **531**, A12
- Shen, S., Madau, P., Guedes, J., et al. 2013, *ApJ*, **765**, 89
- Shibuya, T., Kashikawa, N., Ota, K., et al. 2012, *ApJ*, **752**, 114
- Slosar, A., Font-Ribera, A., Pieri, M. M., et al. 2011, *JCAP*, **2011**, 001
- Stark, D. P., Ellis, R. S., Chiu, K., Ouchi, M., & Bunker, A. 2010, *MNRAS*, **408**, 1628
- Steidel, C. C., Erb, D. K., Shapley, A. E., et al. 2010, *ApJ*, **717**, 289
- Storrie-Lombardi, L. J., & Wolfe, A. M. 2000, *ApJ*, **543**, 552
- Tang, M., Stark, D. P., Chen, Z., et al. 2023, *MNRAS*, **526**, 1657
- Trainor, R. F., Steidel, C. C., Strom, A. L., & Rudie, G. C. 2015, *ApJ*, **809**, 89
- Trainor, R. F., Strom, A. L., Steidel, C. C., et al. 2019, *ApJ*, **887**, 85
- Urrutia, T., Wisotzki, L., Kerutt, J., et al. 2019, *A&A*, **624**, A141
- Verhamme, A., Schaerer, D., & Maselli, A. 2006, *A&A*, **460**, 397
- Virtanen, P., Gommers, R., Oliphant, T. E., et al. 2020, *NatMe*, **17**, 261
- Wisotzki, L., Bacon, R., Blaizot, J., et al. 2016, *A&A*, **587**, A98
- Wisotzki, L., Bacon, R., Brinchmann, J., et al. 2018, *Natur*, **562**, 229
- Wolfe, A. M., Lanzetta, K. M., Foltz, C. B., & Chaffee, F. H. 1995, *ApJ*, **454**, 698